nature communications

Article

https://doi.org/10.1038/s41467-024-51939-w

Phospholipid scrambling induced by an ion channel/metabolite transporter complex

Received: 15 December 2023

Accepted: 21 August 2024

Published online: 31 August 2024

Check for updates

Han Niu[1,2], Masahiro Maruoka[1,3], Yuki Noguchi[1], Hidetaka Kosako[4] & Jun Suzuki[1,2,3,5]

Cells establish the asymmetrical distribution of phospholipids and alter their distribution by phospholipid scrambling (PLS) to adapt to environmental changes. Here, we demonstrate that a protein complex, consisting of the ion channel Tmem63b and the thiamine transporter Slc19a2, induces PLS upon calcium (Ca^{2+}) stimulation. Through revival screening using a CRISPR sgRNA library on high PLS cells, we identify Tmem63b as a PLS-inducing factor. Ca^{2+} stimulation-mediated PLS is suppressed by deletion of Tmem63b, while human disease-related Tmem63b mutants induce constitutive PLS. To search for a molecular link between Ca^{2+} stimulation and PLS, we perform revival screening on Tmem63b-overexpressing cells, and identify Slc19a2 and the Ca^{2+}-activated K^+ channel Kcnn4 as PLS-regulating factors. Deletion of either of these genes decreases PLS activity. Biochemical screening indicates that Tmem63b and Slc19a2 form a heterodimer. These results demonstrate that a Tmem63b/Slc19a2 heterodimer induces PLS upon Ca^{2+} stimulation, along with Kcnn4 activation.

The asymmetrical distribution of molecules across membranes is a fundamental property of cells. For instance, phospholipids are asymmetrically distributed at the lipid bilayer on the plasma membranes. Phosphatidylserine (PS) and phosphatidylethanolamine (PE) are restricted to the inner side of the plasma membranes, while phosphatidylcholine (PC) and sphingomyelin (SM) are mainly located at the outer layer of the membrane[1–4]. However, in some physiological situations, this asymmetry is quickly altered by phospholipid scrambling (PLS) as cells respond to changes in surroundings or to intrinsic cues; in both cases, the consequence of such scrambling exposes PS to the cell surface. Exposed PS functions as a scaffold for coagulation factors on activated platelets when bleeding occurs[5]. Cell surface PS also functions as an "eat-me signal" for dead cells to be engulfed by phagocytes[6–9]. However, the molecular identity of scramblases was unknown for decades.

Previously, using cDNA library screening, we discovered the ubiquitous scramblases Tmem16F and Xkr8, which induce PLS in the coagulation reaction and the clearance of dead cells, respectively[10–14]. Nevertheless, in the absence of these two proteins in Ba/F3 cells (pro-B cell line), PLS is still induced under high Ca^{2+} ionophore stimulation, suggesting that other PLS systems exist on plasma membranes. To search for such factors, we performed revival screening using a CRISPR sgRNA library, which led to the identification of PLS-inducing factors through the enrichment of sgRNAs by reconstitution of the sgRNA library[15]. As a result, we identified the mechano-sensitive channel Tmem63b[16–19], the thiamine transporter Slc19a2[20], and the Ca^{2+}-activated K^+ channel Kcnn4[21–25] as factors regulating PLS. Importantly, Tmem63b and Slc19a2 form a heterodimer, which is activated upon Ca^{2+} stimulation, together with Kcnn4 activation. Additionally, epilepsy and anemia-related Tmem63b mutations led to continuous PLS activity. These results demonstrate that the ion channel/metabolite transporter complex promotes PLS upon Ca^{2+} stimulation, along with Kcnn4 activation, alterations in which could be responsible for human diseases.

[1]Institute for Integrated Cell-Material Sciences (WPI-iCeMS), Kyoto University, Yoshida-Honmachi, Sakyoku Kyoto, Japan. [2]Graduate School of Biostudies, Kyoto University, Konoe-cho, Yoshida, Sakyoku Kyoto, Japan. [3]Center for Integrated Biosystems, Institute for Biomedical Sciences, Academia Sinica Taipei, Taiwan. [4]Fujii Memorial Institute of Medical Sciences, Institute of Advanced Medical Sciences, Tokushima University, Tokushima, Japan. [5]CREST, Japan Science and Technology Agency, Kawaguchi, Saitama, Japan. e-mail: jsuzuki@icems.kyoto-u.ac.jp

Results

Establishment of high phospholipid-scrambling cells

Tmem16F and Xkr8 have been identified as Ca^{2+}-dependent and caspase cleavage-dependent scramblases, respectively[10,12]. These two scramblases-elicited phospholipid scrambling (PLS) activity can be detected by an uptake of the fluorescent lipid NBD-PC in the pro-B cell line Ba/F3. When cells were stimulated with low concentration (0.5 μM) or high concentration (3.0 μM) of the Ca^{2+} ionophore A23187 in Lipid buffer (HBSS with 1 mM $CaCl_2$ and 1 mM $MgCl_2$) at 4 °C for 10 min, they showed similar PLS activity (Fig.1a top). After deleting both *Tmem16F* and *Xkr8* in Ba/F3 cells (BDKO cells), the PLS activity was greatly inhibited at 0.5 μM A23187 stimulation, indicating that these scramblases, especially Tmem16F, contributed to this process (Fig.1a bottom left). However, when stimulated with 3.0 μM A23187, BDKO cells promoted high PLS activity (Fig.1a bottom right), suggesting the existence of unknown Ca^{2+}-dependent scramblase(s) in BDKO cells. To identify the unknown scramblase(s), we planned to isolate a cell population with high PLS activity by a repeated sorting approach[10,15]. BDKO cells were stimulated with 0.5 μM A23187, applied to a PC uptake assay, used to collect high PC uptake cells with flow cytometry, and expanded for the next round of sorting (Fig.1b). After repeating this process for a total of 19 times, we obtained high PLS cells, hPC19, that exhibited PLS activity even in response to 0.5 μM of A23187 (Fig.1c). PLS activity can be examined not only by PC uptake, but also by phosphatidylserine (PS) exposure[10]. When stimulated with 3.0 μM A23187 in Annexin buffer (10 mM HEPES (pH7.4), 140 mM NaCl, 2.5 mM $CaCl_2$) at room temperature, PS exposure in parental BDKO cells reached maximum within 10 min, while that in hPC19 cells reached maximum within 4 min (Fig.1d), confirming successful generation of high PLS cells.

Identification of Tmem63b as a PLS-inducing protein

Next, we sought to perform a CRISPR/Cas9 sgRNA library screening using hPC19 cells to find factors involved in Ca^{2+}-dependent PLS. In particular, we decided to apply a revival screening approach where critical sgRNAs can be identified through reconstitution of an enriched sgRNA library to prevent targets loss due to growth defects possibly caused by the target sgRNAs[15]. As shown in Fig. 2a, hPC19 cells were infected with lentiviral sgRNA library, applied to the PC uptake assay, and subjected to flow cytometry for sorting of PC uptake-negative cells. After genomic (g) DNA purification from the sorted cells, PCR was performed using the purified gDNA to amplify the sgRNA-encoding region. Subsequently, the enriched sgRNA libraries were generated by inserting the amplified PCR products into the lentiviral vector, followed by the next round of screening. After three rounds of sgRNA screening (sgPC3) using enriched sgRNA library, approximately 23% of PC uptake-defective cells were collected and analyzed by next-generation sequencing (NGS) and mapping (Fig.2b). In this sgRNA library, six sgRNAs in average were designed for each gene, and identified sgRNAs containing more than three target sgRNAs among six ones were presented as the total count of mapped targets: the sum of sgRNAs for mapped targets was displayed as a total read and ranked based on the obtained read counts (Fig.2c, Supplemental Data 1). As a

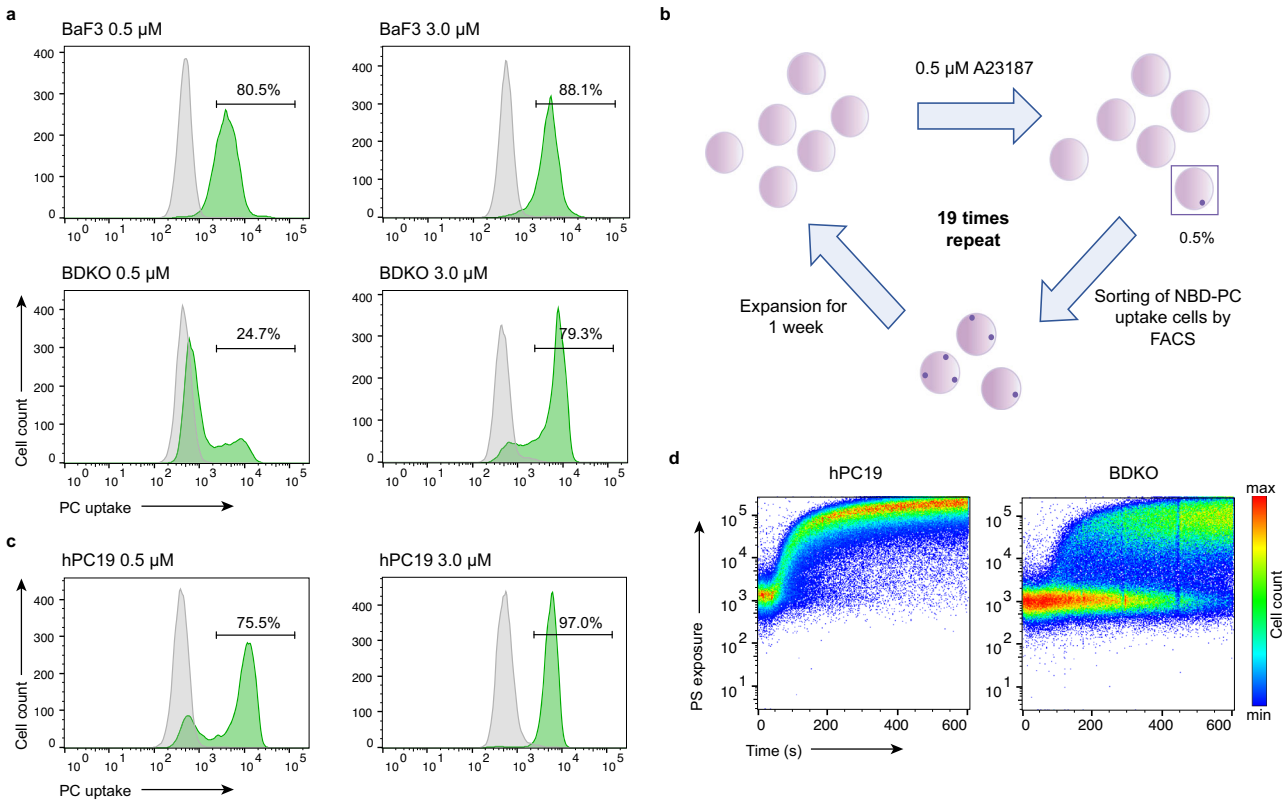

Fig. 1 | Establishment of high PLS cells by repetitive sorting. a Analysis of PLS activity. PLS activity was examined using the NBD-PC uptake assay in Ba/F3 cells and those deficient in Tmem16F and Xkr8 (BDKO cells). Cells were resuspended in Lipid buffer (HBSS with 1 mM $CaCl_2$ and 1 mM $MgCl_2$), stimulated with low A23187 (0.5 μM) and high A23187 (3.0 μM) at 4 ˚C, and analyzed at 0 min (Grey) and 10 min (Green). Bar, PC uptake-positive region; number, cell population in the bar. Experiments were performed independently three times, and representative data is shown. **b** Strategy for establishing high PLS cells. BDKO cells with high NBD-PC uptake activity, when stimulated with A23187 (0.5 μM) in Lipid buffer, were collected by flow cytometry and then expanded. High PLS cells (hPC19) were obtained by sorting repeated 19 times. **c** PC uptake assay in hPC19 cells. hPC19 cells were stimulated with low A23187 (0.5 μM) and high A23187 (3.0 μM) in Lipid buffer at 4 ˚C and analyzed at 0 min (Grey) and 10 min (Green). Bar, PC uptake-positive region; number, cell population in the bar. **d** PS exposure activity. Parental BDKO cells and hPC19 cells were stimulated with 3.0 μM A23187 at room temperature for 10 min in Annexin buffer (10 mM Hepes, 140 mM NaCl, 2.5 mM $CaCl_2$) with Annexin V-Cy5/PI. PI-negative region is shown. Experiments were performed independently three times, and representative data is shown.

https://doi.org/10.1038/s41467-024-51939-w

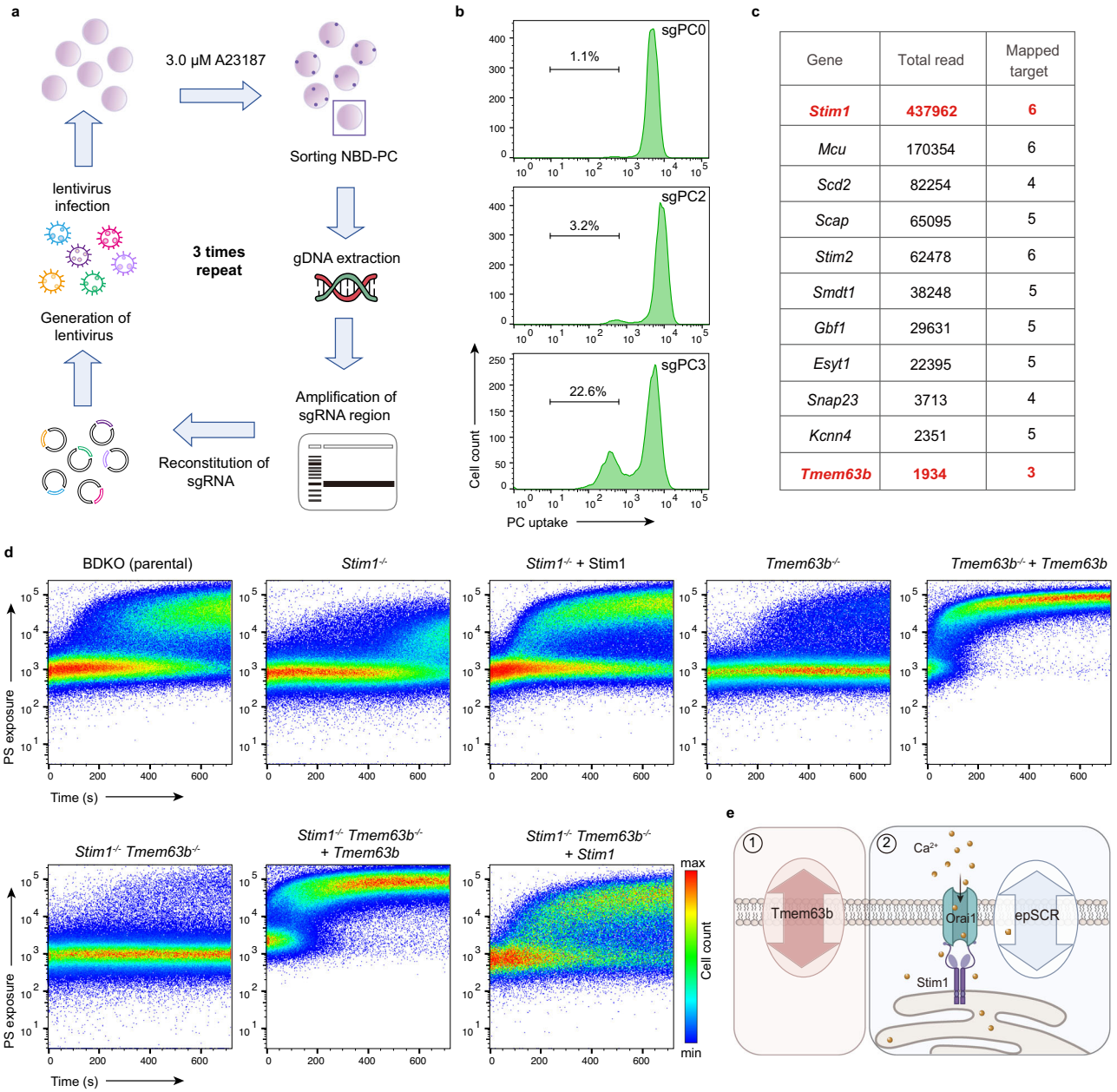

Gene	Total read	Mapped target
Stim1	**437962**	**6**
Mcu	170354	6
Scd2	82254	4
Scap	65095	5
Stim2	62478	6
Smdt1	38248	5
Gbf1	29631	5
Esyt1	22395	5
Snap23	3713	4
Kcnn4	2351	5
Tmem63b	**1934**	**3**

Fig. 2 | Identification of Tmem63b as a PLS-inducing protein. a Schematic representation of revival screening with sgRNA library. sgRNA library was introduced into hPC19 cells expressing CRISPR-Cas9. When performed NBD-PC assay, cells were stimulated by 3.0 μM A23187 in Lipid buffer at 4 °C for 10 min, and PC uptake-negative region was sorted by flow cytometry. From sorted cells, genomic DNA was purified and applied to PCR for amplifying the integrated sgRNA region, followed by inserting into lentiviral vector to reconstitute the enriched sgRNA library. The newly reconstituted library was used for the next round of screening. These processes were repeated 3 times for Next Generation Sequencing (NGS) analysis. **b** Revival screening. PC uptake-negative cells (1%) were sorted by flow cytometry and used for sgRNA library reconstitution. sgPC0, original sgRNA-library introduced cells; sgPC2, cells sorted twice; sgPC3, cells sorted three times. Bar, PC uptake-negative region; number, cell population in the bar. **c** NGS analysis of sgRNAs after fourth sorting. Total reads (sum of reads from different sgRNAs against the same gene) were ranked. Mapped numbers indicate the numbers of identified sgRNA targets among 6 different sgRNAs. Mapped numbers 0 to 2 were eliminated from the list. Genes analyzed further are shown in bold with red color. **d** PLS activity by AnnexinV-Cy5/PI staining was performed in BDKO cells as control, *Stim1* knockout (KO) BDKO cells and those restored with Stim1, *Tmem63b* KO BDKO cells, and those restored with Tmem63b, *Stim1/Tmem63b* double KO BDKO cells and those restored with Tmem63b or Stim1, stimulated with 3.0 μM A23187 in Annexin buffer with AnnexinV-Cy5/PI at room temperature for 10 min. PI-negative region was analyzed. Experiments were performed independently three times, and representative data is shown. **e** A model for two independent Ca^{2+}-mediated PLS systems. 1. Tmem63b-dependent PLS at PM. 2. Stim1/Orai1-dependent PLS at ER-PM contact site. epSCR: unknown ER-PM scramblase.

result, Stim1 ranked top with the highest reads and 6-mapped targets. Stim1 is known as a single transmembrane region-containing protein located at the endoplasmic reticulum (ER), interacting with the Ca^{2+} channel Orai1 on the plasma membranes (PM) to mediate Ca^{2+} influx[26]. To investigate whether Stim1 is associated with the PLS activity, sgRNA against *Stim1* was introduced in parental BDKO cells and a knockout clone was generated (Supplemental Fig. 1a). Consequently, deletion of *Stim1* resulted in delayed PS exposure, compared to parental BDKO cells when stimulated with A23187 (Fig. 2d top second left). Exogenous expression of Stim1 into *Stim1*$^{-/-}$ BDKO cells restored PS exposure (Fig. 2d top middle), demonstrating that Stim1 contributes to Ca^{2+}-dependent PLS. Conversely, Stim1 itself is obviously not a scramblase

on the plasma membranes because it exclusively localizes to the ER. We then questioned which molecule is a potential candidate for the scramblase. From our NGS results, we focused on one multi-transmembrane region-containing protein, localized at the plasma membranes, called Tmem63b (CSC1-like protein), that has been suggested to function as a mechano-sensitive cation channel[16]. Although amino acid sequences are different between Tmem63b and Tmem16 family members, Tmem63b bears highly structural similarity to the Tmem16 family[27], which consists of both ion channels and scramblases[28,29], implying that Tmem63b promotes PLS among its multiple functions. To validate this hypothesis, sgRNA against *Tmem63b* was introduced into BDKO cells and a knockout clone was obtained (Supplemental Fig. 1b). As a result, PS exposure was greatly reduced in *Tmem63b*$^{-/-}$ BDKO cells (Fig.2d top second right) but was rescued with exogenous expression of Tmem63b (Fig.2d top right). It is noted that deletion of *Stim1* or *Tmem63b* did not cause a significant change in calcium influx mediated by A23187 (Supplemental Fig. 1c). Among the Tmem63 family consisting of 3 members, Tmem63b exhibited the strongest PLS activity in *Stim1*$^{-/-}$ cells, compared to Tmem63a and Tmem63c (Supplemental Fig.1d). This result also implied that Tmem63b does not require Stim1 for its activation.

In order to examine whether Stim1 is dispensable in Tmem63b-mediated PLS, *Stim1*$^{-/-}$ and *Tmem63*b$^{-/-}$ BDKO cells were established. Although *Stim1*$^{-/-}$ and *Tmem63*b$^{-/-}$ BDKO cells rarely exhibited PS exposure and PC incorporation (Fig.2d bottom left, Supplemental Fig. 1e), expression of exogenous Tmem63b induced high PS exposure and PC incorporation activities (Fig.2d bottom middle, Supplemental Fig. 1e), demonstrating that Tmem63b promotes Ca^{2+}-dependent PLS without Stim1. Similarly, the introduction of exogenous Stim1 into *Stim1*$^{-/-}$ and *Tmem63*b$^{-/-}$ BDKO cells promoted PLS activity, indicating that Stim1-induced PLS does not require Tmem63b (Fig.1d bottom right, Supplemental Fig. 1e).

When *Orai1* was deleted in *Stim1*$^{-/-}$ and *Tmem63*b$^{-/-}$ BDKO cells restored with Stim1, PS exposure was inhibited while exogenous expression of wild-type (WT), but not the severe combined immunodeficiency-derived mutant R91W[30], rescued the phenotype (Supplemental Fig. 2a), suggesting that Orai1-mediated Ca^{2+} influx at the ER-PM contact site is critical for Stim1-dependent PLS. Indeed, real-time imagining by super-resolution microscopy showed that PS exposure initiated at the ER-PM contact site where Stim1-tagRFP was enriched and spread to whole cells afterward (Supplemental Fig. 2b). This result indicates that A23187 induces Ca^{2+}-release from ER as previously reported, followed by promotion of store-operated Ca^{2+} entry[31,32].

On the other hand, another ER-PM contact site protein, E-syt1[33] or SNARE proteins such as Snap23 and Stx4a[34] (identified by revival screening), were not significantly involved in Stim1-dependent PLS unlike Orai1 (Supplemental Fig. 3a), suggesting that Stim1-dependent PLS requires an unknown PLS-inducing factor (here, we defined it as an endoplasmic reticulum-plasma membrane scramblase, epSCR) at plasma membranes. When these proteins (*Orai1, E-syt1, Snap23, and Stx4a*) were deleted in Tmem63b-expressing *Stim1*$^{-/-}$ and *Tmem63*b$^{-/-}$ BDKO cells, they did not cause significant change in PLS (Supplemental Fig. 3b). Taken together, these results indicate that there are two additional pathways for PLS, expanding beyond the known pathways of Tmem16 and Xkr: Tmem63b-dependent PLS and Stim1/Orai1-mediated epSCR-dependent PLS (Fig. 2e). For further analyses in this study, we focused on Tmem63b-mediated PLS more than Stim1/Orai1-dependent one.

High PLS activity by disease mutants of Tmem63b

According to a recent report[35], TMEM63B is mutated in patients with severe developmental and epileptic encephalopathy (DEE), intellectual disability, severe motor and cortical visual impairment, and progressive neurodegeneration in the brain (Supplemental Fig. 4a). Additionally, most patients' symptoms are accompanied by hematological abnormalities such as macrocytosis and hemolytic anemia[35]. Currently, ten distinct variants of TMEM63B mutations have been identified in 16 patients. The original amino acids of mutant V44M, R433H, D459E, I475del, and R660T, are well conserved among several species (Fig.3a). It is noteworthy that most mutations are in the transmembrane regions of the protein (Fig.3b). To investigate whether these mutations affect the PLS activity, we expressed the mutants in *Tmem63b*$^{-/-}$ BDKO cells and examined their activity. According to previous results, Tmem63b-expressing BDKO cells exhibited PS exposure in less than 1 min at room temperature after A23187 stimulation (Fig.2d), given this time constraint, it is difficult to compare the PLS activity between WT and mutants. To overcome this issue, temperature was decreased to 4°C to delay the reaction speed (Supplemental Fig. 4b). Although Tmem63b WT failed to expose PS without Ca^{2+} ionophore stimulation, most of the Tmem63b variants exhibited continuous PS exposure even without stimulation (Fig.3c top, Fig.3d) which was further enhanced by the stimulation with 3.0 μM A23187 (Fig.3c bottom). Intriguingly, the degree of PLS activity is highly correlated with the severity of hematological disorders. For instance, mutants causing high PLS activity, I475del, and V44M, show severe hemolytic anemia, while moderate PLS activity-inducing mutants, D459E and R660T, lead to mild macrocytic anemia[35], suggesting that these mutants are gain-of-function mutants with different degrees in their activity. On the other hand, one mutant, R433H, that displays abnormalities in red blood cells but fails to cause anemia in patients (Supplemental Fig. 4a), resulted in no PLS activity with or without Ca^{2+} ionophore stimulation (Fig.3c). When localization of the R433H was examined, it localized at the plasma membranes, suggesting that the R433H mutant lost PLS activity because of a loss of function, but not of a change in localization. Although TMEM63B is reported to work as a cation channel to permeate Ca^{2+}[16,19,36], chelating Ca^{2+} by BAPTA-AM had only minor effects on PS exposure activity in Tmem63b mutants-expressing cells (Supplemental Fig. 5), suggesting that Tmem63b-mediated ion flux is not a major factor to induce PLS. Considering that the same concentration (1 μM) of BAPTA-AM completely inhibits Tmem16F mutants-induced PLS[10], we can conclude that BAPTA-AM is sufficient to chelate Ca^{2+} at resting condition.

In order to examine the cell lineage that expresses *TMEM63B*, single cell RNAseq analysis was performed using a public database (E-MTAB-9389) of human fetal bone marrow[37]. As a result, *TMEM63B*, but not *TMEM63A* and *TMEM63C*, were found to be expressed highly in the erythroid lineage, especially in mid and late erythroid. Considering those patients with anemia harbor TMEM63B mutations, dysregulation of TMEM63B in red blood cells may be associated with anemia (Fig. 3e, Supplemental Fig. 6).

Identification of Tmem63b co-factors to induce PLS

Although Tmem63b is activated under Ca^{2+} stimulation, a molecular link between Ca^{2+} influx and Tmem63b activation is missing. To identify factors involved in Tmem63b activation, revival screening using a sgRNA library was performed in Tmem63b-overexpressing BDKO cells. After 3 rounds of sorting for a PS exposure-negative population after A23187 stimulation at 4 °C, PLS-negative cells were enriched up to 16.3% (Fig. 4a). Then gDNA was prepared from collected cells and applied to the NGS analysis, followed by mapping. The candidates were ranked by the number of total reads in mapped targets, and the top three candidates, Csnk2b, Kcnn4, and Slc19a2 were selected for further analysis (Fig.4b, Supplemental Data 2). Csnk2b is a serine/threonine kinase known for phosphorylating many substrates within the cytoplasm. Kcnn4 is a Ca^{2+}-activated K^+ channel on plasma membranes, mutations in which are involved in hereditary xerocytosis[38]. Slc19a2 is a thiamine transporter located on the plasma membranes, defects in which cause thiamine-responsive megaloblastic anemia (TRMA)[39]. In contrast to Fig. 2C, Stim1 was detected at a much lower

https://doi.org/10.1038/s41467-024-51939-w

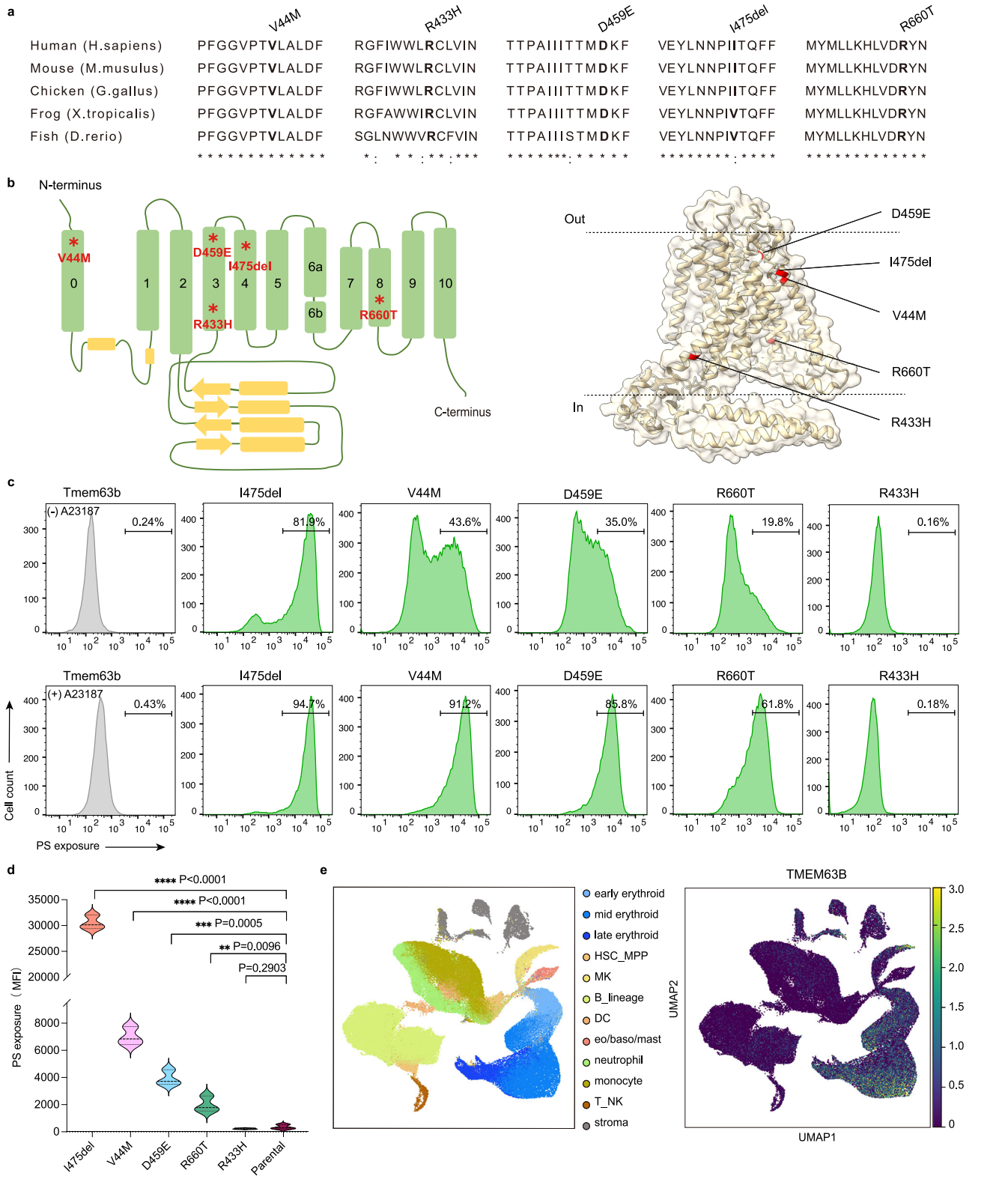

level in total reads (Fig.4b), further demonstrating that Tmem63b-mediated PLS is distinct from Stim1-mediated PLS.

sgRNAs against these three candidates were introduced into Tmem63b-expressing BDKO cells. Especially, decrease in Kcnn4 expression was confirmed at a protein level by BN-PAGE and at an mRNA level by RT-PCR (Supplemental Fig. 7a). Similarly, down-regulation of *Slc19a2* expression level was confirmed at an mRNA level by RT-PCR. As a result, PLS activity evoked by Tmem63b was significantly inhibited under deletion of *Kcnn4* and *Slc19a2* but not that of *Csnk2b* (Fig. 4c–e), suggesting that Kcnn4 and Slc19a2 contribute to the Tmem63b-mediated PLS. Expression of Kcnn4 WT, but not the histidine phosphorylation mutant H358N in the calmodulin-binding domain[40,41], into *sgKcnn4*-introduced *Tmem63b*-expressing BDKO cells rescued the phenotype, suggesting that functional Kcnn4 is involved in induction of Tmem63b-mediated PLS (Fig. 4c, e, Supplemental Fig. 7b). To examine the involvement of Kcnn4 further, Na^+ was replaced with

Fig. 3 | Tmem63b mutants-mediated PLS. a Multiple sequence alignment of Tmem63b and its orthologues in five different vertebrate species (Homo sapiens NP_001305721.1, Mus musculus NP_937810.2, Gallus gallus NP_001366170.1, Xenopus tropicalis XP_031757905.1, Danio rerio NP_001313336.1), with the mutated residues in bold. The asterisk below the sequences shows positions where amino acids were conserved across different species. The colon indicates similar amino acids were conserved across different species. **b** Location of the identified disease mutants (V44M, R433H, D459E, I475del, R660T) on a schematic representation and structure of human TMEM63B protein (pdb: 8ehx). Bold Red, mutations; asterisk, positions of mutations. **c** PS exposure assay. Tmem63b mutants-expressing cells were stimulated with (bottom) or without (top) 3.0 μM A23187 in Annexin buffer with Annexin V-Cy5/PI, incubated at 4 °C for 10 min. Grey, Tmem63b WT-expressing cells. Green, indicated mutants-expressing cells. Bar, PS exposure positive region; number, cell population in the bar. Tmem63b mutant data are displayed according to their strength in activity. **d** Quantification of PS exposure. Mean fluorescence intensity (MFI) of Tmem63b variants without A23187 stimulation in (**c**) is shown as an average of triplicates ($n = 3$, independent experiments). The lines in the middle, bottom, and top indicate median, minimum, and maximum values, respectively. Tmem63b mutant data were displayed according to their strength in activity. Source data are provided as a Source Data file. **e** Uniform manifold approximation and projection (UMAP) of Human fetal bone marrow single cell RNA-seq data ($n = 9$, different BM samples, $k = 103{,}228$, 12–19 post conception weeks (PCW)) was acquired from the database E-MTAB-9389 and analyzed by broad categories. Baso basophil; eo eosinophil; MK megakaryocyte. *TMEM63B* was expressed in erythroid lineages, especially at high level in mid and late erythroid.

K^+ in the extracellular buffer to delay the speed of K^+ efflux. As a result, PS exposure in Tmem63b-expressing cells was decreased in a K^+ concentration-dependent manner (Supplemental Fig. 8a–c). At 4 °C, the effect of extracellular K^+ on PS exposure initiation was obvious than room temperature because the ATP1a1-mediated K^+ influx is likely inhibited, rendering PS exposure more responsive to K^+ efflux. Additionally, ATP-dependent flippases activity is negligible at low temperature, enhancing the sensitivity of PS exposure initiation by the scramblase. Compared to these, at room temperature, we observed that the initiation (0–100 s) and termination (620–720 s) of PS exposure were decreased by increasing extracellular K^+, particularly above at 50 mM K^+, but not affected at 5 mM K^+ (unlike at 4 °C), suggesting that Kcnn4-mediated K^+ efflux is important in the physiological condition to promote Tmem63b-induced PLS. This interpretation is also supported by the drug experiment: treating cells with the Kcnn4 inhibitors Senicapoc and TRAM-34[42,43] significantly blocked Tmem63b-mediated PLS both at 4 °C and at room temperature (Supplemental Fig. 9a, b).

When Slc19a2 was restored in *sgSlc19a2*-introduced *Tmem63b*-expressing BDKO cells, the phenotype was rescued, or rather enhanced (Fig. 4d, e), confirming that Slc19a2 is involved in Tmem63b-mediated PLS. As for the TRMA-related Slc19a2 mutant S143F, it showed weaker PLS activity than Slc19a2 WT in Tmem63b-expressing cells (Fig. 4d, e), suggesting that functional Slc19a2 is critical to induce PLS. When Slc19a2 WT, but not Slc19a2 S143F, was overexpressed into Tmem63b mutants-expressing cells, PLS activity was strongly enhanced (Fig. 4f bottom, Fig. 4g, and Supplemental Fig. 10a), while knockout of *Slc19a2* in Tmem63b mutants-expressing cells greatly reduced the PLS activity (Fig. 4f second bottom and Fig. 4g). Conversely, Kcnn4 overexpression or deletion did not change the activity significantly (Fig. 4f, h), suggesting that Tmem63b mutants do not require Kcnn4 for its activation. This result is consistent with the high PLS activity observed in Tmem63b mutants-expressing cells even after addition of extracellular high K^+ (Supplemental Fig. 10b). Taken together, these results demonstrated that Slc19a2 and Kcnn4 play important roles for Tmem63b WT-mediated PLS, but Kcnn4 is dispensable for constitutive PLS induced by Tmem63b mutants.

Tmem63b forms a heterodimer with Slc19a2

Based on the known activation mechanisms of identified scramblases, Tmem16, and Xkr family members, dimer formation is critical to induce PLS. Tmem16F generates homodimers in resting and activated states[44–46], while the Xkr family members Xkr4 and Xkr8 form a homodimer after caspase-mediated cleavage[14,15]. In the case of Tmem63b, it has been known that it mainly exists as a monomer[16–19]. Indeed, Blue Native-PAGE (BN-PAGE) analysis showed a predominant monomer-like band, with a less prominent dimer-like band (Fig. 5a). To search for components in the dimer-like band, we performed immunoprecipitation and mass spectrometry analysis, and found that Slc19a2, which we identified by revival screening (Fig. 4b), was precipitated with Tmem63b (Fig. 5b, Supplemental Data 3). Indeed, when Tmem63b-GFP was co-expressed with Slc19a2, but not with Kcnn4 or Csnk2b, the dimer-like band became much stronger (Fig. 5c). To confirm that Tmem63b and Slc19a2 form a heterodimer, a gel shift assay was performed. Tmem63b-FLAG-GFP and Slc19a2-HA were expressed in BDKO cells, from which cell lysates were prepared and incubated with anti-FLAG or anti-HA antibodies, followed by BN-PAGE analysis. When cell lysates were incubated with the anti-FLAG antibody, both monomer and dimer bands were shifted, confirming that these two bands contain Tmem63b (Fig. 5d left). On the other hand, when cell lysates were incubated with the anti-HA antibody, only the dimer band was shifted, indicating that this band contains both Tmem63b and Slc19a2 (Fig. 5d right). When Tmem63b-GFP was co-expressed with both Kcnn4-HA and Slc19a2-FLAG, a dimer band appeared. This band was shifted with anti-FLAG antibody, but not by anti-HA antibody, suggesting that Kcnn4 is not involved in this complex and Tmem63b and Slc19a2 form a heterodimer (Supplemental Fig. 11a). Supporting this idea, amounts of the Tmem63b/Slc19a2 heterodimer were not decreased by deleting *Kcnn4* (Supplemental Fig. 11b). To examine whether the Tmem63b/Slc19a2 complex formation is essential for PLS activity, we tried to identify amino acids at the interface using AlphaFold2. Through mutating the 5 hydrophobic amino acids at the interface (F213 and L217 on TM2, and M711, F712, and I719 on TM10) to Alanine (Supplemental Fig. 12a, b), significant decrease in PLS activity was observed in Tmem63b Ala-expressing BDKO cells (Supplemental Fig. 12c, e). It is noteworthy that Tmem63b Ala localized at the plasma membranes (Supplemental Fig. 12d). In consistent with PLS activity, complex formation was disrupted in Tmem63b Ala-expressing cells (Supplemental Fig. 12f), demonstrating that the heterodimer formation between Tmem63b and Slc19a2 is indispensable to induce PLS.

Next, we asked whether disease-derived mutants of Tmem63b affect the complex formation. When Tmem63b mutants were expressed in cells, the dimer band was slightly, but not significantly, increased compared to Tmem63b WT (Fig. 5e) and this was greatly increased after expression of Slc19a2 WT (Fig. 5f). It is noteworthy that the dimer and monomer ratio is well correlated with the PLS activity induced by Tmem63b mutants (Fig. 3c). Although overexpression of Slc19a2 WT increased heterodimer formation in Tmem63b mutants-expressing cells (Fig. 5f), compared to that with endogenous Slc19a2 (Fig. 5e), overexpression of the anemia-related mutant Slc19a2 S143F did not increase the dimer significantly (Fig. 5g), compared to that with Slc19a2 WT (Fig. 5f). It is noted that, among Tmem63B mutants, an I475del mutant showed the strongest activity and could form more heterodimer even with Slc19a2 S143F. These results suggested that functional Slc19a2 is important for a heterodimer formation with Tmem63b. This tendency is observed even using Tmem63b WT, and the presence of Ca^{2+} or EGTA did not affect the heterodimer formation and PLS activity (Fig.5h), suggesting that the heterodimer is formed without Ca^{2+} stimulation.

https://doi.org/10.1038/s41467-024-51939-w

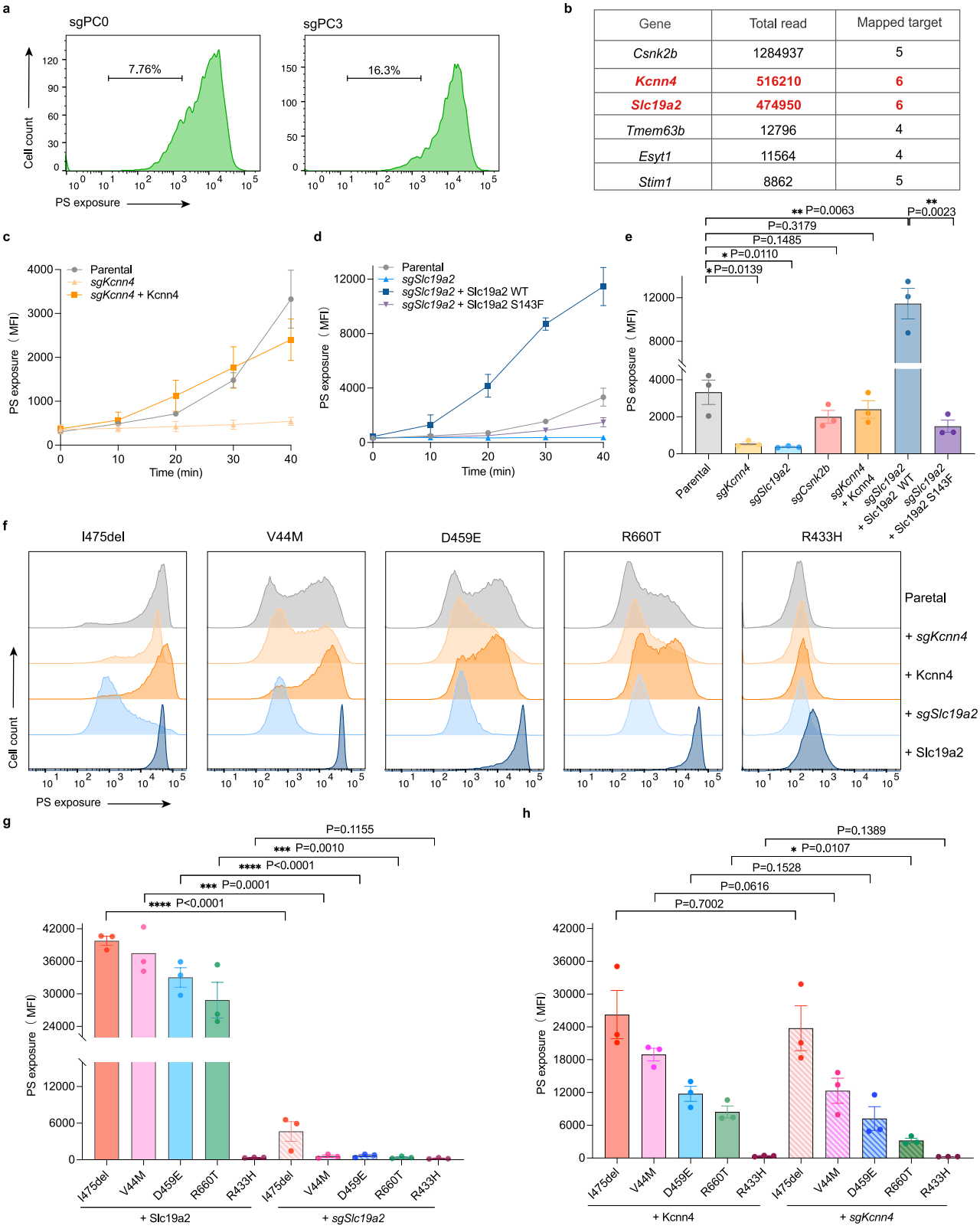

Gene	Total read	Mapped target
Csnk2b	1284937	5
Kcnn4	**516210**	**6**
Slc19a2	**474950**	**6**
Tmem63b	12796	4
Esyt1	11564	4
Stim1	8862	5

From these observations, we describe a model for Tmem63b/Slc19a2-induced PLS. 1. Tmem63b and Slc19a2 form a heterodimer. 2. Ca^{2+} stimulation activates Kcnn4. 3. Upon Kcnn4-mediated K^+ efflux, the Tmem63b/Slc19a2 heterodimer executes PLS. 4. Disease-related mutants of Tmem63b induce PLS activity independently of Kcnn4-mediated K^+ efflux (Fig. 5i).

Discussion

Here, we show that there are two Ca^{2+}-induced PLS pathways in Ba/F3 cells other than the known PLS pathways requiring Tmem16 and Xkr. Stim1 binds to Orai family members at the PM-ER contact site, indicating that Orai-mediated Ca^{2+} influx at the microenvironment induces PLS. Although the PLS-inducing protein epSCR was not identified in

Fig. 4 | Identification of activators for Tmem63b-mediated PLS. a Revival screening. Tmem63b-GFP-expressing BDKO cells were stimulated with 3.0 μM A23187 in Annexin buffer with Annexin V-Cy5/PI at 4 °C for 1 h and subjected to flow cytometry to collect PS exposure-negative cells among the GFP-positive population and used for reconstitution of the enriched sgRNA library. sgPC0, original sgRNA-library introduced cells; sgPC3, cells sorted three times. Bar, PS exposure-negative region; number, cell population in the bar. **b** NGS analysis after fourth sorting. Total reads (sum of reads from different sgRNAs against the same gene) were ranked. Mapped numbers indicate the numbers of identified sgRNA targets among 6 different sgRNAs. Mapped numbers 0 to 2 were eliminated from the list. Genes analyzed further are shown in bold with red color. **c** PS exposure assay. Tmem63b-GFP-expressing BDKO cells and those expressing *sgKcnn4* and both *sgKcnn4* and Kcnn4 WT-tagRFP were stimulated with 3 μM A23187 in Annexin buffer containing AnnexinV-Cy5/PI at 4 °C. Flow cytometry analysis was conducted every 10 min. PI-negative cells were analyzed. The average in triplicates ($n = 3$, independent experiments) is shown with an error bar. Data are presented as mean values ± SEM. Source data are provided as a Source Data file. **d** PS exposure assay. Tmem63b-GFP-expressing BDKO cells and those expressing *sgSlc19a2* and both *sgSlc19a2* and Slc19a2 WT-tagRFP or S143F-tagRFP were stimulated with 3.0 μM A23187 in Annexin buffer containing AnnexinV-Cy5/PI at 4 °C. Flow cytometry analysis was conducted every 10 min. PI-negative cells are shown. The average in triplicates ($n = 3$, independent experiments) is shown with an error bar. Data are presented as mean values ± SEM. Source data are provided as a Source Data file. **e** Comparison of (**c** and **d**). The average of PS exposure at 40 min is shown. Data are presented as mean values ± SEM. Statistical analysis was performed using a two-tailed Student's t-test. $p < 0.05$ was considered statistically significant. *$p < 0.05$, **$p < 0.01$. Source data are provided as a Source Data file. **f** PS exposure assay. Indicated Tmem63b mutants-GFP-expressing cells with Slc19a2-tagRFP or *sgSlc19a2*, and Kcnn4-tagRFP or *sgKcnn4* were incubated in Annexin Buffer with AnnexinV-Cy5/PI at 4 °C for 10 min without A23187 stimulation. **g**, **h** Quantification of (**f**). Experiments were performed independently 3 times and averages of PS exposure are shown with an error bar. Data are presented as mean values ± SEM. Statistical analysis was performed using a two-tailed Student's t-test. $p < 0.05$ was considered statistically significant. *$p < 0.05$, ***$p < 0.001$, ****$p < 0.0001$. The columns for cells expressing both Tmem63b mutants and *sgRNAs* were shaded. Source data are provided as a Source Data file.

this report, future study will reveal how the Stim1/Orai1 pathway promotes PLS at the membrane contact site. In contrast, Tmem63b-mediated PLS was shown to be independent of the Stim1/Orai1 pathway. The Tmem63b protein was found to form a heterodimer with Slc19a2 to promote PLS. Previously, Tmem16 family proteins were shown to form homodimers[44–46]. Xkr proteins also form a homodimer when cleaved at their C-terminus by caspases[14,15,47]. Although the plant orthologue of Tmem63, OSCA forms a homodimer, Tmem63b is likely to form a heterodimer with Slc19a2, which is then activated by Ca^{2+}-mediated simulation of Kcnn4 to execute PLS. Significantly, the epilepsy and anemia-related mutant Tmem63b proteins[35] form more heterodimers, displaying constitutive PLS without Kcnn4 activation. It is interesting to speculate that the ion channel Tmem63b changes its properties as a channel or PLS-inducing protein depending on its cellular context.

Currently, PLS activity of Tmem63b mutants (Figs. 3c, 4f) exhibits a strong correlation with dimer formation between Tmem63b and Slc19a2 WT (Fig. 5f). When Tmem63b mutants were expressed with Slc19a2 S143F, PLS activity was reduced (Supplemental Fig. 10a) with less dimer formation (Fig. 5g), compared to Slc19a2 WT-expressing cells. PLS activity of Tmem63b WT (Fig. 4d) is also associated with dimer formation (Fig. 5h). Based on these observations, we conclude that Tmem63b/Slc19a2 heterodimer formation is significant to induce PLS. Indeed, the heterodimer model, predicted by Alphafold2 (Supplemental Fig. 12a, b), and the subsequent Tmem63b Ala mutants' analysis showed that the heterodimer formation is critical to induce PLS (Supplemental Fig. 12c–e). Future study will be expected to reveal the dimer interface through structural analysis.

Tmem63 family proteins (Tmem63a, Tmem63b, and Tmem63c) are known to mainly exist as monomers and exhibit mechanosensitive channel activity[17–19]. Tmem63b is activated through Ca^{2+}-mediated activation of Kcnn4 and therefore is most likely to be indirectly Ca^{2+}-dependent. At present, it is unknown how Tmem63b forms a heterodimer with Slc19a2. Considering that functional Slc19a2 is required for heterodimer formation with Tmem63b, Slc19a2-mediated transport of substrates such as thiamine may promote heterodimer formation. Kcnn4 has been known to contribute to PS exposure in red blood cells as a Gardos channel[21–23]. It is most likely that Kcnn4 activates the Tmem63b and Slc19a2 complex to execute PLS in red blood cells. We hypothesize that Ca^{2+}-dependent K^+ efflux, facilitated by Kcnn4, led to water efflux along with cell shrinkage[48] and contributes to Tmem63b/Slc19a2-mediated PS exposure. Previous studies have shown that in red blood cells, Ca^{2+} stimulation induces K^+ efflux, leading to cell shrinkage and PS exposure[49,50]. However, the mechanism of Tmem63b activation in this context remains unclear. One possible interpretation of our data is that Ca^{2+}-dependent K^+ efflux triggers water efflux and cell shrinkage, which subsequently activates Tmem63b by altering membrane tension. Recent findings suggest that hyperosmolality-mediated water efflux activates Tmem63b in specific neurons[36]. Based on this, we propose that Tmem63b is activated through sensing changes in membrane tension, particularly membrane compaction.

Conversely, a few studies have reported that hypo-osmolarity-mediated cell swelling or membrane stretch can activate Tmem63b-mediated ion channel activity[16,35]. If membrane stretch primarily activates stretch-dependent channels such as Piezo1, leading to Ca^{2+} influx, Ca^{2+}-dependent Kcnn4 could be activated to induce K^+ efflux. These sequential events might activate Tmem63b through membrane compaction, which would subsequently turn off Piezo1-mediated Ca^{2+} influx as a negative feedback mechanism. In human genetic diseases, gain-of-function mutations in both *PIEZO1* and *KCNN4* are linked to xerocytosis of red blood cells[38,51–53], supporting the hypothesis that Piezo1 and Kcnn4 function within the same pathway. This needs to be investigated in future studies.

Lastly, through this research, we introduce the notion that heterodimers composed of proteins with independent functions exhibit the emergent ability to induce PLS, contrasting with the previously identified PLS proteins, Tmem16 and Xkr, which form homodimers to induce PLS activity.

Methods

Cell culture

HEK293T cells were cultured in the DMEM (WAKO) containing 10% Fetal Bovine Serum (FBS) (Gibco) and 1% Penicillin-Streptomycin solution (Nacalai). Mouse pro-B cell line Ba/F3 cells deficient for *Xkr8* and *Tmem16F* (BDKO cells) and its derivatives were maintained in RPMI 1640 (WAKO) containing 10% FBS (Gibco), 1% Penicillin-Streptomycin solution, 45 units/ml IL-3 (as prepared before[10,54]), and 55 μM 2-mercaptoethanol (Gibco). Cells were maintained in a culture incubator set at 37 °C, supplied with 5% CO_2 at 90–95% humidity.

Plasmid preparation

cDNAs for Tmem63a (NCBI_accession no. NM_001417552.1), Tmem63b (NCBI_accession no. NM_001413622.1), Tmem63c (NCBI_accession no. NM_001361704.1), Slc19a2 (NCBI accession no. NM_054087.3), Kcnn4 (NCBI_accession no. NM_001163510.2), Stim1 (NCBI_ accession no. NM_001374058.1), Orai1 (NCBI_accession no. NM_175423.3), and Csnk2b (NCBI_accession no. NM_001303445.1) were amplified by PCR using cDNA from BDKO cells. The amplified cDNAs were C-terminally tagged with GFP, tagRFP (Evrogen), FLAG, HA, FLAG-GFP, or HA-tagRFP, then inserted into the lentivirus vector (plenti)[15] using the In-Fusion system (Takara) and sequenced. Mutants of Tmem63b were

https://doi.org/10.1038/s41467-024-51939-w

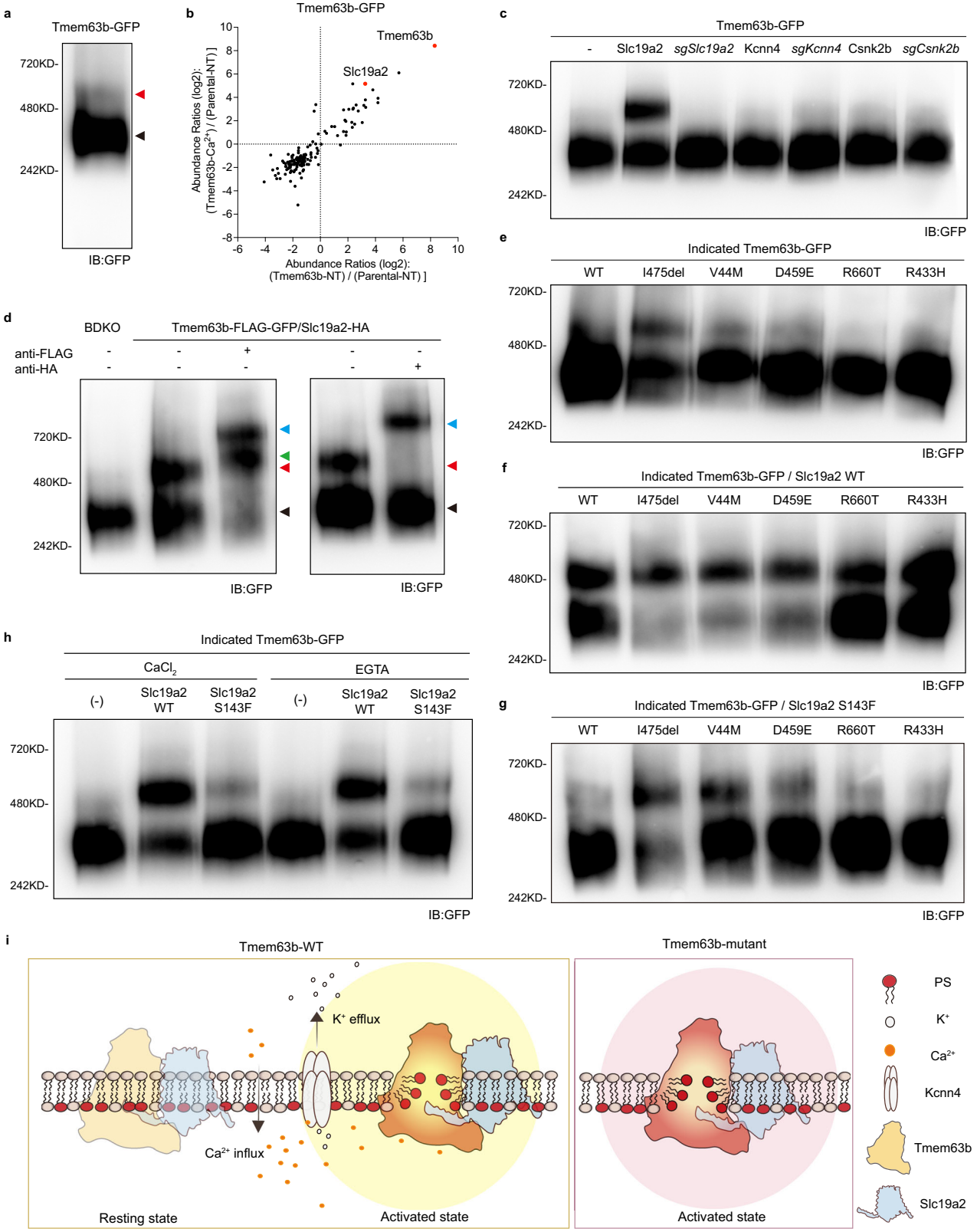

generated by amino acid substitution as following: Valine at 44 was substituted with Methionine (V44M), Arginine at 433 was substituted with Histidine (R433H), Aspartic acid at 459 was substituted with Glutamic acid (D459E), Isoleucine at 475 was deleted (I475del) and Arginine at 660 was substituted with Threonine (R600T). The Tmem63b/Slc19a2 interface mutant of Tmem63b (F213A, L217A, M711A, F712A, and I719A) were generated by replacing each amino acid with Alanine. An Slc19a2 mutant was generated by amino acid substitution: Serine at 143 was substituted with Phenylalanine (S143F). A Kcnn4 mutant: Histidine at 358 was substituted with asparagine (H358N). An Orai1 mutant: Arginine at 91 was substituted with tryptophan (R91W). These mutants were generated by the In-Fusion system using cDNA for each gene and inserted into the plenti vectors, followed by Sanger sequencing.

Fig. 5 | Tmem63B and Slc19a2 form a heterodimer. a BN-PAGE analysis of lysate from Tmem63b GFP-expressing BDKO cells. Tmem63b mainly exists as a monomer (black arrowhead) and slightly as a dimer-like state (red arrowhead). Anti-GFP was used to detect Tmem63b. Experiments were performed independently three times, and representative data is shown. **b** Tmem63b interactors. Tmem63b GFP-expressing cells were solubilized by LMNG/CHS and applied to immunoprecipitation using anti-GFP nanobody-conjugated beads, followed by mass spectrometry. x axis, abundance ratios shown in fold change (log2) between Tmem63b and parental cells without Ca^{2+}; y axis, abundance ratios shown in fold change (log2) between Tmem63b and parental cells with Ca^{2+}. Red dot, Tmem63b, and Slc19a2. **c** BN-PAGE analysis of Tmem63b-expressing cells with Slc19a2-tagRFP, Kcnn4-tagRFP and Csnk2b-tagRFP overexpression, or *sgSlc19a2, sgKcnn4* and *sgCsnk2b* introduction. Anti-GFP was used to detect Tmem63b. Experiments were performed independently three times and representative data is shown. **d** BN-PAGE analysis of Tmem63b-FLAG-GFP-expressing cells with Slc19a2-HA-tagRFP overexpression. After solubilization by detergent, cell lysate was mixed with anti-FLAG or anti-HA antibodies and applied to BN-PAGE to observe the gel shift. Black, monomer; Red, heterodimer; Green, monomer with antibody; Blue, heterodimer with antibody. Anti-GFP was used to detect Tmem63b. Experiments were performed twice, and representative data is shown. **e** BN-PAGE analysis of Tmem63b mutant-expressing cells. Anti-GFP was used to detect Tmem63b. Experiments were performed independently three times and representative data is shown. **f** BN-PAGE analysis of Tmem63b mutant-expressing cells with Slc19a2 WT-tagRFP overexpression. Anti-GFP was used to detect Tmem63b. Experiments were performed independently three times and representative data is shown. **g** BN-PAGE analysis of Tmem63b mutant-expressing cells with Slc19a2 S143F-tagRFP overexpression. Anti-GFP was used to detect Tmem63b. **h** BN-PAGE analysis of Tmem63b-expressing cells with Slc19a2 WT-tagRFP or S143F-tagRFP overexpression in the presence of 1 mM $CaCl_2$ or 0.5 mM EGTA. Anti-GFP was used to detect Tmem63b. Experiments were performed independently twice, and representative data is shown. **i** Schematic model of Tmem63b/Slc19a2-mediated PLS. In activated state, Ca^{2+} stimulation induced Tmem63b/Slc19a2 heterodimer-mediated PLS, along with Kcnn4 activation (left). In Tmem63b mutant-expressing cells, continuous PLS occurs without Ca^{2+} stimulation or K^+ efflux (right).

Establishment of KO cell line

sgRNA was designed using cDNA sequence of target gene as an input in CRISPRdirect (https://crispr.dbcls.jp/) and specific sgRNAs with fewer off-target were selected. Following the protocol described by the Zhang Lab, restriction enzyme sites for BsmBI were attached to sgRNA oligos to insert the annealed oligos into lentiGuide-Puro vector[55] (Addgene#52963). sgRNAs against mouse Tmem63b (5′-CGGAGGT GAGACGCTCATAC-3′), mouse Stim1 (5′-CATCGTCATCCATCAGCTTA-3′), mouse Slc19a2 (5′-AGGGCAGATCCTCGTCTCCG-3′), mouse Kcnn4 (5′-TGCGGTAGGACGCGTTGAGC-3′), mouse Csnk2b (5′-CCAGAGCGA CTTGATCGAAC-3′), mouse E-syt1 (5′-CTTTAGCCATTACGAATCAT-3′), mouse Orai1 (5′-CCTCAACGAGCACTCGATGC-3′), mouse Snap23 (5′-GATTACAAATGGTCAGCCTC-3′), and mouse Stx4a (5′-GCTGTTTGA TCTCCTCTCGC-3′) were designed and inserted into the lentiviral vectors by ligation. To check knockout efficiency, gDNA was extracted using the gDNA extraction kit (Viogene), from which sgRNA target site-containing region was amplified by PCR. The amplified PCR products, corresponding to around 400 bp, were excised from agarose gel, purified, and checked by the Sanger sequencing. For rescue experiments in sgRNA-introduced cells, silence mutations were introduced into the target site of each gene so that the inserted lentiviral sgRNA cannot target the exogenous cDNA.

Lentiviral production

To generate lentiviruses, lentiGuide-Puro vectors or plenti vectors encoding each gene, pCAG HIV-Gag-Pol (RIKEN), and pCMV VSVG-RSV-REV (RIKEN) were transfected into HEK293T cells using the Polyethylenimine (PEI) system (Polysciences). Two days after transfection, supernatant was collected, passed through 0.22 μm filter and centrifuged (6000 × *g*, 4 °C, for 16 h). The viral pellet from 10 ml culture medium was then resuspended in 500 μl RPMI medium containing IL-3 with 10 μg/ml polybrene (Nacalai) to generate 20× concentrated viruses and incubated with cells in the well of 24 well plate. After 6 h incubation, the medium was changed, and cells were expanded. When sgRNA was introduced, 1 μg/ml puromycin (InvivoGen) was added to culture medium one day after viral infection. The drug-containing medium was subsequently replaced with fresh medium after 2 days treatment.

NBD-PC uptake assay

Briefly, 1×10^6 BDKO cells were collected and washed with chilled Lipid buffer (HBSS buffer containing 1 mM $MgCl_2$ and 1 mM $CaCl_2$), incubated in Lipid buffer on ice for 7 min, treated with 1 μM NBD-PC (Avanti, 810132 C) on ice for 3 min, then stimulated with 3.0 μM A23187 (Sigma, C7522). After A23187 stimulation for indicated periods, cells were incubated with Lipid buffer containing 5 mg/ml fatty acid (FA)-free BSA (Sigma, A6003) and 1 μM DAPI (Dojindo) on ice for 5 min to remove NBD-PC locating at the outer layer of membranes. The NBD-PC uptake was examined by flow cytometry such as FACS Lyric and FACS AriaII (Beckton Dickinson).

For revival screening based on NBD-PC uptake, 4×10^7 cells were wash by 20 ml chilled Lipid buffer, incubated in 10 ml Lipid buffer on ice for 7 min, mixed and incubated with 10 ml Lipid buffer containing 1 μM NBD-PC on ice for 3 min. After 3.0 μM A23187 stimulation for 10 min, the reaction was stopped by adding 20 ml Lipid buffer containing 5 mg/ml FA-free BSA and 1 μM DAPI, and incubated on ice for 5 min, followed by centrifugation (400 × *g*, 2 min, 4 °C) and resuspension in 5 ml Lipid buffer for flow cytometry analysis.

PS exposure assay

Briefly, 1×10^6 BDKO cells were washed with PBS and resuspended in 1 ml Annexin buffer (10 mM HEPES-NaOH (pH7.4), 140 mM NaCl, 2.5 mM $CaCl_2$) containing 1000-fold diluted AnnexinV-Cy5 (Biovision) and 1 μg/ml Propidium iodide (PI, Dojindo). Cells were then stimulated with 3.0 μM A23187 and PS exposure was examined at room temperature by flow cytometry for time course analysis. In some cases, PS exposure analysis was performed on ice to delay the speed of PS exposure. For this analysis, cells were washed with chilled PBS and resuspended in chilled Annexin buffer containing AnnexinV-Cy5 and PI, followed by stimulation with 3.0 μM A23187. The stimulated cells were incubated on ice and PS exposure was measured every 10 min.

For revival screening based on PS exposure, 4×10^7 cells were washed by 10 ml chilled PBS, resuspended in 20 ml chilled Annexin buffer containing AnnexinV-Cy5 and PI, incubated at 4 °C for 1 h, centrifuged (400 × *g*, 4 °C, for 5 min), resuspended in 5 ml Annexin buffer (used for the reaction) and applied to cell sorting by flow cytometry.

To observe the effect of extracellular K^+ on PS exposure, NaCl in Annexin buffer was changed to varied concentration of KCl (0 mM, 0.5 mM, 5 mM, 50 mM, or 140 mM). For drug treatment, cells were suspended in Annexin buffer, incubated with the Kcnn4 inhibitors TRAM-34 (10 μM, Selleck) and Senicapoc (0.5 μM, Selleck) at room temperature or 4 °C for 4 min, followed by Ca^{2+} ionophore stimulation and PS exposure analysis.

Establishment of high PLS cells

To establish high PLS cells from BDKO cells, Cas9-expressing BDKO cells were applied to repeated sorting. Briefly, 4×10^7 cells were washed and resuspended in Lipid buffer (HBSS with 1 mM $CaCl_2$ and 1 mM $MgCl_2$), followed by addition of Lipid buffer containing 1 μM NBD-PC and incubation with 0.5 μM A23187 in 10 °C water bath for 8 min.

After the reaction, cells were mixed with 20 ml Lipid buffer containing 5 mg/ml FA-free BSA and 1 μM DAPI on ice for 5 min, then applied to sorting with flow cytometry. Sorted cells were collected into RPMI medium containing IL-3 and 0.5 mM EGTA. The next day, the medium was changed to normal RPMI medium containing IL-3, and cells were expanded for the next sorting. After repeating these processes for 19 times, high PLS cells (hPC19) were established.

Revival screening

hPC19 cells expressing Cas9 were infected with lentiviral sgRNA library (GeCKO v2 Mouse CRISPR Knockout Pooled Library[55]). In 4 days after infection, cells were applied to the NBD-PC uptake assay. Each time, around 1% NBD-PC uptake-negative cells were sorted by flow cytometry and applied to gDNA purification. Then purified gDNA was used to amplify the integrated sgRNA region by PCR using a primer set described below.

sgRNA FW: GTTTTAAAATGGACTATCATATGC

sgRNA RV: TATCCATCTTTGCACCCGGGC

The PCR band was excised from agarose gel, and mixed with lentiviral vectors digested with SmaI and NdeI (NEB), followed by NEBuilder® HiFi DNA Assembly (NEB) at 52 °C for 1 h. Subsequently, the mixture was introduced into MegaX DH10B T1R Electrocomp™ Cells (Invitrogen) through electroporation, followed by 2 h incubation in SOC medium at 32 °C, and then spread onto LB agar plates. The clone number of the resulting library was verified by counting the colonies, where the number is expected to be more than 1×10^6. The enriched sgRNA library was then used for the next round of screening. After repeating these processes 3 times, PC uptake-negative cells were enriched and used to amplify the inserted sgRNA from purified gDNA, followed by the next generation sequencing (NGS) analysis and mapping. Tmem63b-overexpressing BDKO cells with Cas9 were similarly applied to revival screening.

Next generation sequencing

sgRNA regions inserted into gDNA were amplified by PCR using primers described below.

FW PCR primer: GTTTTAAAATGGACTATCATATGC

RV PCR primer: TATCCATCTTTGCACCCGGGC

Obtained PCR products were then applied to the 2nd PCR to add adapter sequences using primers described below.

Adapter FW:

AATGATACGGCGACCACCGAGATCTACACTCTTTCCCTACACGA CGCTCTTCCGATCTATCGACTCTTGTGGAAAGGACGAAACACCG

Adapter RV: CAAGCAGAAGACGGCATACGAGATTCTACTATTCT TTCCCCTGCACTGT

The amplified PCR products were then purified and sent to Macrogen for the Illumina HiSeq2500 analysis.

sgRNA data processing

The sgRNA sequences were analyzed by guide-caller v1.0.0 (https://github.com/SuzukiLab-icems/guide-caller/tree/main/v1.0.0)[56]. This tool utilizes a standard analysis framework comprising FastQC (https://www.bioinformatics.babraham.ac.uk/projects/fastqc/), Cutadapt[57], and MAGeCK[58]. Specifically, the 20 bp sgRNA sequences were isolated from the 51 bp sequenced reads by employing Cutadapt for dual-round trimming, with the parameters "-u 30" for the initial trim and "-u -1" for the subsequent trim. The resulting trimmed reads were then aligned with MAGeCK to a modified annotation list[56].

Fluo4-AM Assay

1×10^6 cells were incubated with 1 μM Fluo4-AM (Dojindo) in culture medium at 37 °C for 30 min. Then, cells were centrifuged (400 × *g*, RT, for 2 min), followed by washing and resuspending in Annexin buffer. The cells were then loaded onto flow cytometry (FACS Lyric) and recorded. Approximately 100 seconds later, 3.0 μM A23187 was added into the sample, and cells were recorded for another 50 s to detect changes in Ca^{2+} influx.

BAPTA-AM Assay

1×10^6 cells were incubated with 1 μM BAPTA-AM (Dojindo) in culture medium at 37 °C for 30 min. Then, cells were centrifuged (400 × *g*, 4 °C, for 2 min), washed, and resuspended in Annexin buffer. The cells were either treated with or without 3.0 μM A23187 in Annexin buffer at 4 °C before being loaded onto flow cytometry (FACS Lyric) and recorded.

High resolution live-cell imaging of PS exposure

High resolution imaging of Stim1-mediated PLS activity was observed by an Airyscan super-resolution confocal microscopy (Zeiss, LSM980). Briefly, 5×10^5 cells were washed and resuspended at room temperature in 500 μl Annexin buffer containing 1000-fold diluted DAPI and AnnexinV-Cy5, then stimulated with 3.0 μM A23187. The cells were immediately seeded in glass bottom chambers coated with 50 μg/mL Poly-L-lysin (Sigma, P2636). Image acquisition was started 90 s after cell seeding and images were acquired every 30 s for 10 min using a 63×/1.46 NA oil immersion Plan-Apochromat objective with Zeiss Airyscan 2 detector module. During imaging, cells were maintained at 25 °C. After imaging, cell survival was judged by checking the DAPI signal.

Identification of TMEM63B-positive fetal bone marrow cells

Cell types expressing TMEM63B in human fetal bone marrow were identified through a reanalysis of the 10x single-cell RNA sequencing (scRNA-seq) dataset "fig1b_fbm_scaled_gex_updated_dr_20210104.h5ad." This data underwent normalization and scaling processes. Subsequently, more detailed cell type annotations were conducted, and the re-annotated cells were depicted as UMAP with expressions of these genes following the methodology described by Jardine et al[37].

(https://github.com/haniffalab/FCA_bone_marrow/blob/master/fig1_fbm_disomic_and_trisomy21/fig1a_suppfig1b_fbm_overall_dr_plots_SW.ipynb).

Cell lysate preparation

A total of 1×10^6 BDKO cells were harvested and washed twice with cold PBS. Subsequently, they were centrifuged (400 × *g*, 4 °C, for 2 min), resuspended in solubilization buffer (25 mM Tris-HCl (pH 8.0), 100 mM 6-aminocaprotic acid, 140 mM NaCl, 1% Lauryl Maltose Neopentyl Glycol (LMNG, Anatrace, NG310) /Cholesteryl hemisuccinate (CHS, Sigma, C6512) at a ratio of 10:1, 10% (vol/vol) Glycerol, 1 mM p-APMSF (Nacalai), EDTA-free protease inhibitor cocktail (Nacalai), 1 mM NaF, 2 mM DTT), and rotated at 4 °C for 1 h. The solubilized lysate was then applied to centrifugation (20,000 × *g*, 4 °C, 20 min) to remove insoluble materials.

Membrane fraction preparation

For preparation of membrane fraction, 2×10^7 cells were washed twice with cold PBS then homogenized using a Dounce homogenizer in a hypotonic buffer (25 mM Tris-HCl (pH 8.0), 10 mM $MgCl_2$, 20 mM KCl, 250 mM Sucrose, 1 mM p-APMSF, protease inhibitor cocktail (Nacalai), 1 mM NaF, and 2 mM DTT). Then adding equal amount of Isotonic buffer (25 mM Tris-HCl (pH 8.0), 200 mM NaCl, 10 mM $MgCl_2$, 20 mM KCl, 250 mM Sucrose, 1 mM p-APMSF, protease inhibitor cocktail (Nacalai), 1 mM NaF, and 2 mM DTT). After removing nuclei (800 × *g*, 4 °C, for 10 min) and mitochondria (8000 × *g*, 4 °C, for 10 min), the supernatant was applied to ultracentrifugation (100,000 × *g*, 4 °C, 1 h). The pellet was collected and solubilized with solubilization buffer (25 mM Tris-HCl (pH 8.0), 100 mM 6-aminocaprotic acid, 140 mM NaCl, 1% LMNG/0.1% CHS, 10% (vol/vol) Glycerol, 1 mM p-APMSF (Nacalai), EDTA-free protease inhibitor cocktail (Nacalai), 1 mM NaF,

2 mM DTT for 2 h, followed by centrifugation (20,000 × *g*, 4 °C, 20 min) to remove the insoluble materials and protein quantification.

BN-PAGE analysis

Before loading the obtained lysate to the Blue Native (BN)-PAGE Novex Bis-Tris gel (Life Technologies), lysate concentration was measured by Bradford assay kit (Thermo Fisher Scientific, 23246) and adjusted to 0.5 mg/ml using the solubilization buffer. In some cases, cell lysates were incubated with anti-DDDDK antibody (MBL, PM020) or anti-HA.11 Epitope Tag antibody (Biolegend, 16B12) on ice for 1 h to perform the gel shift assay before loading to the BN-PAGE Bis-Tris gels. Then loaded proteins were separated by electrophoresis at 150 V for 35 min at 4 °C in cathode buffer concludes 0.02% CBB G-250. After running for 35 min, the cathode buffer was changed to one containing 0.002% CBB G-250 and run at 150 V for 120 min. After electrophoresis, the gel was incubated with SDS running buffer (25 mM Tris-HCl, 190 mM Glycine, 0.1% SDS) at room temperature for 20 min, then transferred to the Immobilon-P PVDF membrane (Millipore) at 100 mA for 1 hr, and applied to western blotting.

Western blotting

After BN-PAGE analysis, proteins were transferred to the Immobilon-P PVDF membrane by running at 100 mA for 1 h, applied to blocking with 5% skim milk in TBS-T (50 mM Tris-HCl, 300 mM NaCl, 0.05% Tween20), and incubated with the indicated antibody. The anti-GFP-HRP antibody (MBL, 598-7) was used at 6000-fold dilution or anti-Kcnn4 antibody (Proteintech, 23271-1-AP) was used at 2000-fold dilution and incubated overnight at 4 °C while shaking. After washing with TBST for 5 min 4 times, goat anti-rabbit IgG HRP (DAKO) was applied at 10000-fold dilution and incubated at room temperature for 1 h to detect Kcnn4. Subsequently, the membrane was washed 4 times with TBST, followed by detection of chemiluminescent signal using Immobilon Western chemiluminescent HRP substrate (Millipore) through the FUSION chemiluminescence imaging system (Vilber). PVDF membrane was stained by CBB staining buffer (0.25% CBB R250, 50% methanol, 10% acetic acid), then washed with destaining buffer (30% methanol and 10% acetic acid). An obtained band was used for normalizing the loading amount.

Real-time PCR

RNA was extracted from 1×10^6 cells using the RNeasy kit (Qiagen, 74104), followed by conversion into cDNA using the High-Capacity RNA-to-cDNA Kit (Thermo Fisher Scientific, 4387406). Primers for the target genes were designed by the Primer-BLAST.

Mouse *Kcnn4* FW: 5′-GCAAGATTGTCTGCCTGTGC-3′
Mouse *Kcnn4* RV: 5′-TCTCCGCCTTGTTGAACTCC-3′
Mouse *Slc19a2* FW: 5′-ATGAGCCTCCGGTGGAAGAA-3′
Mouse *Slc19a2* RV: 5′-GGGCGGGAGGAATAACACAT-3′
Mouse *Actin* FW: 5′-GGCTGTATTCCCCTCCATCG-3′
Mouse *Actin* RV: 5′-CCAGTTGGTAATGCCATGT-3′

RNA expression levels were assessed utilizing the Comparative Ct Method (ΔΔCt method). Based on averaged Ct values, the fold change in expression of *Kcnn4* or *Slc19a2* in *sgKcnn4*- or *sgSlc19a2*-expressing BDKO cells compared to parental BDKO cells was analyzed, then normalized to the internal control *(Actin* gene) in quantitative real-time PCR reaction (RT-PCR) performed by Takara Thermal Cycler Dice Real Time System Lite using TB Green Premix Ex Taq™ II (Tli RNaseH Plus) (TAKARA).

Immunoprecipitation and mass spectrometry

4×10^6 cells (BDKO and Tmem63b-GFP-expressing BDKO, n = 1) were collected, washed twice by PBS, and incubated with 0.1% formaldehyde at room temperature for 10 min, followed by 1 M glycine-NaOH incubation for 4 min. After centrifugation and PBS wash, cells were resuspended in 500 μl solubilization buffer (25 mM Tris-HCl (pH 8.0), 140 mM NaCl, 1% LMNG/0.1% CHS, 10% (vol/vol) Glycerol, 1 mM p-APMSF, EDTA-free protease inhibitor cocktail (Nacalai), 100 mM 6-aminocaprotic acid, 1 mM NaF, 2 mM DTT) with or without 1 mM $CaCl_2$ and in the presence of 1/500 Benesonase, and rotated at 4 °C for 1 h. Then, supernatant was collected after centrifugation (20,000 × *g*, 4 °C, 20 min) and applied to incubation with GFP-Trap magnetic agarose beads (Proteintech). Beads were equilibrated with solubilization buffer twice before incubation with cell lysate and were rotated at 4 °C for 3 h with cell lysate. Then, beads were precipitated with magnetic rack, washed with 500 μl washing buffer (25 mM Tris-HCl (pH 8.0), 100 mM 6-aminocaprotic acid, 140 mM NaCl, 0.01% LMNG/0.001% CHS) for 3 times, and washed with 50 μl 50 mM Ammonium Bicarbonate for another 2 times. Samples were flash frozen with liquid nitrogen and kept at −80 °C until use. Subsequently, proteins bound to the beads were digested by adding trypsin/Lys-C mix (Promega) at 37 °C for 16 h, after which the resulting digested products were used for a series of steps including reduction, alkylation, acidification, and desalting using GL-Tip SDB (GL Sciences). The eluates were concentrated in a SpeedVac concentrator, followed by dissolution in a solution consisting of 0.1% trifluoroacetic acid and 3% acetonitrile (ACN). LC-MS/MS analysis of the generated peptides was executed on an EASY-nLC 1200 UHPLC connected to an Orbitrap Fusion mass spectrometer via a nanoelectrospray ion source (Thermo Fisher Scientific). The separation of peptides occurred on a 75 μm inner diameter × 150 mm C18 reversed-phase column (Nikkyo Technos), using a linear 4–32% ACN gradient over 0–100 min, followed by a 10 min increase to 80% ACN. The mass spectrometer was operated in a data-dependent acquisition mode, with a maximum duty cycle of 3 s. MS1 spectra were measured with a resolution of 120,000, an automatic gain control (AGC) target of 4×10^5, and a mass range from 375 to 1500 *m/z*. HCD MS/MS spectra were acquired in the linear ion trap with an AGC target of 1×10^4, an isolation window of 1.6 *m/z*, a maximum injection time of 100 ms, and a normalized collision energy of 30. Dynamic exclusion was set to 20 s. The raw data were directly analyzed against the SwissProt database restricted to *Mus musculus* using Proteome Discoverer version 2.5 (Thermo Fisher Scientific) with the Sequest HT search engine. The search parameters included trypsin as the enzyme with up to two missed cleavages, a minimum peptide length of 6 amino acids, a precursor mass tolerance of 10 ppm, a fragment mass tolerance of 0.6 Da, carbamidomethylation of cysteine as a fixed modification, and acetylation of the protein N-terminus and oxidation of methionine as variable modifications. Peptides were filtered at a false-discovery rate of 1% using the percolator node. Label-free precursor ion quantification was conducted using the precursor ions quantifier node, and normalization was performed to ensure that the total sum of abundance values for each sample over all peptides remained consistent.

Prediction of Tmem63b/Slc19a2 heterodimer

Structure of Tmem63b mutant (V44M) and Slc19a2 heterodimer were predicted using AlphaFold2[59] (v 2.3.2) through the AlphaFold ColabFold v1.5.5 implementation with default settings and Amber relaxation (msa_method = mmseqs2_uniref_env, pair_mode = unpaired_paired, model_type = auto, num_recycles = 3, recycle_early_stop_tolerance = auto, relax_max_iterations = 200, pairing_strategy = greedy, max_msa = auto, num_seeds = 1, dpi = 200, rank_num = 1, color = IDDT). AlphaFold2 generated 5 trained models after a single run and calculated the pLDDT, pTM and ipTM scores which indicate the accuracy of the prediction. The model with a high score (pLDDT = 69.9, pTM = 0.575, ipTM = 0.331) was selected for analyzing the interface of Tmem63b mutant and Slc19a2. All views of structures were analyzed using the ChimeraX software. Computation time was provided by the Supercomputer System at Institute for Chemical Research, Kyoto University.

Statistics and reproducibility. Student's t-test (unpaired t-test) was used for statistical analysis. Experiments for quantitative analysis of PLS activity were performed independently three times and qualitative confirmation was performed twice. BN-PAGE analysis was mostly performed independently three times, or twice in some cases (e.g., gel shift assay). For PLS assay, we used 1×10^6 cells for the assay to ensure stable handling and consistent results across experiments. We did not apply blinding because value for flow cytometry is objective and quantitative, and interpretation of data shows no bias. For microscopy analysis, experiments were done independently three times. At each experiment, 3 images comprising of more than 10 cells/image were taken, and the representative data were shown in Figures.

Reporting summary

Further information on research design is available in the Nature Portfolio Reporting Summary linked to this article.

Data availability

CRISPR screening data generated in this study are provided in the Supplementary Information 1 and 2. Mass spectrometry data generated in this study are provided in the Supplementary Information 3 and have been deposited to the ProteomeXchange consortium via the jPOST partner repository with the dataset identifier PXD054885. The Genbank accession codes for genes are as follows: mouse Tmem63a NM_001417552.1 [https://www-ncbi-nlm-nih-gov/nuccore/NM_001417552.1], mouse Tmem63b NM_001413622.1 [https://www-ncbi-nlm-nih-gov/nuccore/NM_001413622.1], mouse Tmem63c NM_001361704.1 [https://www.ncbi.nlm.nih.gov/nuccore/NM_001361704.1], mouse Slc19a2 NM_054087.3 [https://www-ncbi-nlm-nih-gov/nuccore/NM_054087.3], mouse Kcnn4 NM_001163510.2 [https://www-ncbi-nlm-nih-gov/nuccore/NM_001163510.2], mouse Stim1 NM_001374058.1 [https://www-ncbi-nlm-nih-gov/nuccore/NM_001374058.1], mouse Orai1 NM_175423.3 [https://www-ncbi-nlm-nih-gov/nuccore/NM_175423.3], and mouse Csnk2b NM_ 001303445.1 [https://www-ncbi-nlm-nih-gov/nuccore/NM_001303445.1]. The Genbank accession codes for proteins Tmem63b in different species are as follows: human NP_001305721.1 [https://www-ncbi-nlm-nih-gov/protein/NP_001305721.1], mouse NP_937810.2 [https://www-ncbi-nlm-nih-gov/protein/NP_937810.2], chicken NP_001366170.1 [https://www-ncbi-nlm-nih-gov/protein/NP_001366170.1], frog XP_031757905.1 [https://www-ncbi-nlm-nih-gov/protein/XP_031757905.1], fish NP_001313336.1 [https://www-ncbi-nlm-nih-gov/protein/NP_001313336.1]. Accession code for single cell analysis in human fetal bone marrow on BioStudies is E-MTAB-9389. An accession code for human TMEM63B cryo-EM structure is PDB Data Bank with ID number: 8EHX. Source data are provided with this paper.

Code availability

Codes for sgRNA analysis (guide-caller and martrix_shaper for CRISPR screening) and scRNAseq analysis are provided in the Source Data file.

References

1. van Meer, G., Voelker, D. R. & Feigenson, G. W. Membrane lipids: where they are and how they behave. *Nat. Rev. Mol. cell Biol.* **9**, 112–124 (2008).
2. Leventis, P. A. & Grinstein, S. The distribution and function of phosphatidylserine in cellular membranes. *Annu. Rev. Biophys.* **39**, 407–427 (2010).
3. Andersen, J. P. et al. P4-ATPases as phospholipid flippases-structure, function, and enigmas. *Front. Physiol.* **7**, 275 (2016).
4. Pomorski, T. & Menon, A. K. Lipid flippases and their biological functions. *Cell. Mol. Life Sci. CMLS* **63**, 2908–2921 (2006).
5. Zwaal, R. F., Comfurius, P. & Bevers, E. M. Surface exposure of phosphatidylserine in pathological cells. *Cell. Mol. Life Sci. CMLS* **62**, 971–988 (2005).
6. Ravichandran, K. S. Find-me and eat-me signals in apoptotic cell clearance: progress and conundrums. *J. Exp. Med.* **207**, 1807–1817 (2010).
7. Bevers, E. M. & Williamson, P. L. Getting to the outer leaflet: physiology of phosphatidylserine exposure at the plasma membrane. *Physiol. Rev.* **96**, 605–645 (2016).
8. Nagata, S. Apoptosis and clearance of apoptotic cells. *Annu. Rev. Immunol.* **36**, 489–517 (2018).
9. Maruoka, M. & Suzuki, J. Regulation of phospholipid dynamics in brain. *Neurosci. Res.* https://doi.org/10.1016/j.neures.2021.01.003 (2021).
10. Suzuki, J., Umeda, M., Sims, P. J. & Nagata, S. Calcium-dependent phospholipid scrambling by TMEM16F. *Nature* **468**, 834–838 (2010).
11. Suzuki, J. et al. Calcium-dependent phospholipid scramblase activity of TMEM16 protein family members. *J. Biol. Chem.* **288**, 13305–13316 (2013).
12. Suzuki, J., Denning, D. P., Imanishi, E., Horvitz, H. R. & Nagata, S. Xk-related protein 8 and CED-8 promote phosphatidylserine exposure in apoptotic cells. *Science* **341**, 403–406 (2013).
13. Suzuki, J., Imanishi, E. & Nagata, S. Exposure of phosphatidylserine by Xk-related protein family members during apoptosis. *J. Biol. Chem.* **289**, 30257–30267 (2014).
14. Suzuki, J., Imanishi, E. & Nagata, S. Xkr8 phospholipid scrambling complex in apoptotic phosphatidylserine exposure. *Proc. Natl Acad. Sci. USA* **113**, 9509–9514 (2016).
15. Maruoka, M. et al. Caspase cleavage releases a nuclear protein fragment that stimulates phospholipid scrambling at the plasma membrane. *Mol. Cell* **81**, 1397–1410.e1399 (2021).
16. Du, H. et al. The cation channel TMEM63B is an osmosensor required for hearing. *Cell Rep.* **31**, 107596 (2020).
17. Zhang, M., Shan, Y., Cox, C. D. & Pei, D. A mechanical-coupling mechanism in OSCA/TMEM63 channel mechanosensitivity. *Nat. Commun.* **14**, 3943 (2023).
18. Qin, Y. et al. Cryo-EM structure of TMEM63C suggests it functions as a monomer. *Nat. Commun.* **14**, 7265 (2023).
19. Zheng, W. et al. TMEM63 proteins function as monomeric high-threshold mechanosensitive ion channels. *Neuron* **111**, 3195–3210.e3197 (2023).
20. Diaz, G. A., Banikazemi, M., Oishi, K., Desnick, R. J. & Gelb, B. D. Mutations in a new gene encoding a thiamine transporter cause thiamine-responsive megaloblastic anaemia syndrome. *Nat. Genet.* **22**, 309–312 (1999).
21. Joiner, W. J., Wang, L. Y., Tang, M. D. & Kaczmarek, L. K. hSK4, a member of a novel subfamily of calcium-activated potassium channels. *Proc. Natl Acad. Sci. USA* **94**, 11013–11018 (1997).
22. Ishii, T. M. et al. A human intermediate conductance calcium-activated potassium channel. *Proc. Natl Acad. Sci. USA* **94**, 11651–11656 (1997).
23. Logsdon, N. J., Kang, J., Togo, J. A., Christian, E. P. & Aiyar, J. A novel gene, hKCa4, encodes the calcium-activated potassium channel in human T lymphocytes. *J. Biol. Chem.* **272**, 32723–32726 (1997).
24. Vandorpe, D. H. et al. cDNA cloning and functional characterization of the mouse Ca^{2+}-gated K^+ channel, mIK1. Roles in regulatory volume decrease and erythroid differentiation. *J. Biol. Chem.* **273**, 21542–21553 (1998).
25. Warth, R. et al. Molecular and functional characterization of the small Ca(2+)-regulated K^+ channel (rSK4) of colonic crypts. *Pflug. Arch. Eur. J. Physiol.* **438**, 437–444 (1999).
26. Hogan, P. G. The STIM1-ORAI1 microdomain. *Cell Calcium* **58**, 357–367 (2015).
27. Zhang, M. et al. Structure of the mechanosensitive OSCA channels. *Nat. Struct. Mol. Biol.* **25**, 850–858 (2018).
28. Pedemonte, N. & Galietta, L. J. Structure and function of TMEM16 proteins (anoctamins). *Physiol. Rev.* **94**, 419–459 (2014).

29. Jin, P., Jan, L. Y. & Jan, Y. N. Mechanosensitive ion channels: structural features relevant to mechanotransduction mechanisms. *Annu. Rev. Neurosci.* **43**, 207–229 (2020).
30. Feske, S. et al. A mutation in Orai1 causes immune deficiency by abrogating CRAC channel function. *Nature* **441**, 179–185 (2006).
31. Sun, C. et al. Central role of IP(3)R2-mediated Ca(2+) oscillation in self-renewal of liver cancer stem cells elucidated by high-signal ER sensor. *Cell Death Dis.* **10**, 396 (2019).
32. Preissler, S. et al. Calcium depletion challenges endoplasmic reticulum proteostasis by destabilising BiP-substrate complexes. *eLife* **9**, e62601 (2020).
33. Saheki, Y. et al. Control of plasma membrane lipid homeostasis by the extended synaptotagmins. *Nat. Cell Biol.* **18**, 504–515 (2016).
34. Chen, Y. A. & Scheller, R. H. SNARE-mediated membrane fusion. *Nat. Rev. Mol. Cell Biol.* **2**, 98–106 (2001).
35. Vetro, A. et al. Stretch-activated ion channel TMEM63B associates with developmental and epileptic encephalopathies and progressive neurodegeneration. *Am. J. Hum. Genet.* **110**, 1356–1376 (2023).
36. Yang, F. et al. Single-cell multi-omics analysis of lineage development and spatial organization in the human fetal cerebellum. *Cell Discov.* **10**, 22 (2024).
37. Jardine, L. et al. Blood and immune development in human fetal bone marrow and Down syndrome. *Nature* **598**, 327–331 (2021).
38. Glogowska, E., Lezon-Geyda, K., Maksimova, Y., Schulz, V. P. & Gallagher, P. G. Mutations in the Gardos channel (KCNN4) are associated with hereditary xerocytosis. *Blood* **126**, 1281–1284 (2015).
39. Labay, V. et al. Mutations in SLC19A2 cause thiamine-responsive megaloblastic anaemia associated with diabetes mellitus and deafness. *Nat. Genet.* **22**, 300–304 (1999).
40. Srivastava, S. et al. Phosphatidylinositol 3-phosphate indirectly activates KCa3.1 via 14 amino acids in the carboxy terminus of KCa3.1. *Mol. Biol. Cell* **17**, 146–154 (2006).
41. Srivastava, S. et al. Histidine phosphorylation of the potassium channel KCa3.1 by nucleoside diphosphate kinase B is required for activation of KCa3.1 and CD4 T cells. *Mol. Cell* **24**, 665–675 (2006).
42. Klein, H. et al. Structural determinants of the closed KCa3.1 channel pore in relation to channel gating: results from a substituted cysteine accessibility analysis. *J. Gen. Physiol.* **129**, 299–315 (2007).
43. Rapetti-Mauss, R., Soriani, O., Vinti, H., Badens, C. & Guizouarn, H. Senicapoc: a potent candidate for the treatment of a subset of hereditary xerocytosis caused by mutations in the Gardos channel. *Haematologica* **101**, e431–e435 (2016).
44. Sheridan, J. T. et al. Characterization of the oligomeric structure of the Ca(2+)-activated Cl- channel Ano1/TMEM16A. *J. Biol. Chem.* **286**, 1381–1388 (2011).
45. Suzuki, T., Suzuki, J. & Nagata, S. Functional swapping between transmembrane proteins TMEM16A and TMEM16F. *J. Biol. Chem.* **289**, 7438–7447 (2014).
46. Brunner, J. D., Lim, N. K., Schenck, S., Duerst, A. & Dutzler, R. X-ray structure of a calcium-activated TMEM16 lipid scramblase. *Nature* **516**, 207–212 (2014).
47. Zhang, P. et al. Extracellular calcium functions as a molecular glue for transmembrane helices to activate the scramblase Xkr4. *Nat. Commun.* **14**, 5592 (2023).
48. Begenisich, T. et al. Physiological roles of the intermediate conductance, Ca^{2+}-activated potassium channel Kcnn4. *J. Biol. Chem.* **279**, 47681–47687 (2004).
49. Lang, K. S. et al. Enhanced erythrocyte apoptosis in sickle cell anemia, thalassemia and glucose-6-phosphate dehydrogenase deficiency. *Cell. Physiol. Biochem. Int. J. Exp. Cell. Physiol. Biochem. Pharmacol.* **12**, 365–372 (2002).
50. Lang, P. A. et al. Role of Ca^{2+}-activated K^+ channels in human erythrocyte apoptosis. *Am. J. Physiol. Cell Physiol.* **285**, C1553–1560, (2003).
51. Zarychanski, R. et al. Mutations in the mechanotransduction protein PIEZO1 are associated with hereditary xerocytosis. *Blood* **120**, 1908–1915 (2012).
52. Albuisson, J. et al. Dehydrated hereditary stomatocytosis linked to gain-of-function mutations in mechanically activated PIEZO1 ion channels. *Nat. Commun.* **4**, 1884 (2013).
53. Andolfo, I. et al. Multiple clinical forms of dehydrated hereditary stomatocytosis arise from mutations in PIEZO1. *Blood* **121**, 3925–3935 (2013). s3921-3912.
54. Fukunaga, R., Ishizaka-Ikeda, E. & Nagata, S. Purification and characterization of the receptor for murine granulocyte colony-stimulating factor. *J. Biol. Chem.* **265**, 14008–14015 (1990).
55. Sanjana, N. E., Shalem, O. & Zhang, F. Improved vectors and genome-wide libraries for CRISPR screening. *Nat. Methods* **11**, 783–784 (2014).
56. Noguchi, Y. et al. In vivo CRISPR screening directly targeting testicular cells. *Cell Genomics* **4**, 100510 (2024).
57. Martin, M. Cutadapt removes adapter sequences from high-throughput sequencing reads. *EMBnet.J.* **17**, https://doi.org/10.14806/ej.17.1.200. (2011).
58. Li, W. et al. MAGeCK enables robust identification of essential genes from genome-scale CRISPR/Cas9 knockout screens. *Genome Biol.* **15**, 554 (2014).
59. Jumper, J. et al. Highly accurate protein structure prediction with AlphaFold. *Nature* **596**, 583–589 (2021).

Acknowledgements

We thank T. Ohara for the early stage of this work, S. Kawaguchi for discussion on electrophysiology, E. Alvi for proofreading of the manuscript, and A. Fujimoto for secretarial assistance. This work was supported by Grants-in-Aid for Scientific Research B (KAKENHI 22H02572), Grant-in-Aid for Challenging Research (Exploratory, KAKENHI 21K19261), JST-CREST (1199566), Joint Usage and Joint Research Programs of the Institute of Advanced Medical Sciences of Tokushima University, WPI-iCeMS, Takeda Science Foundation to J. Suzuki.

Author contributions

H. Niu and J. Suzuki designed overall research and interpreted experimental results. H. Niu performed most of the experiments. H. Niu performed the revival screening with help of M. Maruoka. Y. Noguchi performed the NGS analysis. H. Kosako performed mass spectrometry analysis. H. Niu and J. Suzuki wrote the manuscript.

Competing interests

J. Suzuki, H. Niu, and M. Maruoka are inventors on a patent application of Ca^{2+}-dependent phospholipid scrambling. The remaining authors declare no competing interests.

Additional information

Supplementary information The online version contains supplementary material available at https://doi.org/10.1038/s41467-024-51939-w.

Correspondence and requests for materials should be addressed to Jun Suzuki.

Peer review information *Nature Communications* thanks H. Criss Hartzell, and the other, anonymous, reviewer(s) for their contribution to the peer review of this work. A peer review file is available.